Loschmidt echo as a robust decoherence quantifier for many-body systems

Pablo R. Zangara, Axel D. Dente, Patricia R. Levstein, and Horacio M. Pastawski*
Instituto de Física Enrique Gaviola (CONICET) and Facultad de Matemática, Astronomía y Física, Universidad Nacional de Córdoba, 5000 Córdoba, Argentina
(Received 8 November 2011; published 18 July 2012)

We employ the Loschmidt echo, i.e., the signal recovered after the reversal of an evolution, to identify and quantify the processes contributing to decoherence. This procedure, which has been extensively used in single-particle physics, is employed here in a spin ladder. The isolated chains have 1/2 spins with XY interaction and their excitations would sustain a one-body-like propagation. One of them constitutes the controlled system $\mathcal{S}$ whose reversible dynamics is degraded by the weak coupling with the uncontrolled second chain, i.e., the environment $\mathcal{E}$. The perturbative $\mathcal{SE}$ coupling is swept through arbitrary combinations of XY and Ising-like interactions, that contain the standard Heisenberg and dipolar ones. Different time regimes are identified for the Loschmidt echo dynamics in this perturbative configuration. In particular, the exponential decay scales as a Fermi golden rule, where the contributions of the different $\mathcal{SE}$ terms are individually evaluated and analyzed. Comparisons with previous analytical and numerical evaluations of decoherence based on the attenuation of specific interferences show that the Loschmidt echo is an advantageous decoherence quantifier at any time, regardless of the $\mathcal{S}$ internal dynamics.

DOI: 10.1103/PhysRevA.86.012322 PACS number(s): 03.67.Hk, 03.65.Yz, 75.10.Pq

I. INTRODUCTION

The physical realization of quantum information processing (QIP) [1] requires a precise control of quantum dynamics. The coherent manipulation of many-body systems plays a crucial role for several QIP-related implementations, such as spintronic devices [2], optical lattices [3,4], superconducting circuits [5], and nitrogen-vacancy centers in diamond [6]. Experiments with spin arrays in nuclear magnetic resonance (NMR) [7–9] have shown that many-body dynamics conspires against quantum control. Moreover, once the system interacts with an environment, control becomes even more difficult due to information leakage. This degradation of the system's coherent dynamics, called decoherence, is the subject of deep theoretical and experimental investigation [10], as it remains the key obstacle for QIP. Indeed, quantum error correction protocols [11,12] can restore quantum information provided that they operate above a certain threshold. Achieving this limit is often a task for dynamical decoupling techniques [13–15]. However, specific implementations require a precise knowledge of the nature of the decoherence processes [16]. It is the purpose of this paper to contribute to a better characterization of the role of a spin environment in the decoherence of a many-spin system.

At least for short distance communications, spin chains can be used to transfer information [17]. In fact, several selective polarization techniques have been developed in NMR experiments to set up an initial local excitation in one edge of a spin chain and transfer it to the other edge by means of an effective XY Hamiltonian (i.e., $S_i^+ S_j^- + S_i^- S_j^+$ or polarization-conserving "flip-flop" processes) [18,19]. Additionally, multiple quantum coherence spectroscopy has allowed the study of quasi-one-dimensional spin systems under the influence of spin environments [20,21]. Here, the double-quantum Hamiltonian (i.e., the $S_i^+ S_j^+ + S_i^- S_j^-$ processes) can be mapped to an XY Hamiltonian allowing the design and control of the excitation transfer in a broader family of solid-state spin structures [19,22–25]. Thus, a deep knowledge of decoherence in such one-dimensional (1D) systems is crucial to improve the degree of control available for NMR-based state transfer protocols [26,27].

A natural way to quantify the decoherence time τ_ϕ is through the degradation of interferences. This requires the identification of specific coherence "witnesses," such as excitations in the local polarization. Particularly useful are the reflections in the boundaries that can be observed as well-defined mesoscopic echoes (MEs) [28–30]. Recently, the ME intensity has been used to quantify the decoherence of spins arranged in a ladder topology [31]. Alternatively, the evaluation of τ_ϕ can be performed by a time reversal procedure, the Loschmidt echo (LE) [32], where one evaluates the reversibility of the system's dynamics in the presence of an uncontrolled environment. The LE can be accessed experimentally in many situations, such as spin systems [7,8,33], confined atoms [34], and microwave excitations [35]. Besides, it has become a standard way to quantify decoherence, stability, and complexity in dynamical processes, in several physical situations [36,37].

In the present article, we address the controllability of a spin chain ($\mathcal{S}$) in the presence of a spin environment ($\mathcal{E}$) by performing a quantitative study of the LE. LE degradation characterizes the decoherence due to the perturbation of $\mathcal{E}$ on the otherwise simple dynamics of $\mathcal{S}$. Indeed, the many-body nature of the $\mathcal{S}$-$\mathcal{E}$ interaction yields a very rich behavior in the dynamical regimes of decoherence: a short-time quadratic decay, an exponential regime, and a saturation plateau are identified by our numerical approach. In particular, we perform a detailed analysis of LE exponential decay, addressing how the rates scale with a Fermi golden rule (FGR). Additionally, since for weak perturbations the LE of the local excitation can be seen as a survival probability (SP), the numerical results are compared to previous analytical predictions for that magnitude [38].

*horacio@famaf.unc.edu.ar

In the next section, we describe the spin problem and summarize its theoretical background. We introduce the spin autocorrelation function and describe a single-particle analogy which underlies further analysis. We also discuss the local version of the LE and present its definition in terms of the local polarization, which is the usual experimental observable. In Sec. III A, we present the numerical study of the LE for some of the different physically relevant parameters. We consider $\mathcal{S}$-$\mathcal{E}$ interactions which are weak compared with those determining the $\mathcal{E}$ dynamics. We also address different anisotropies of the $\mathcal{S}$-$\mathcal{E}$ interaction which range from pure XY (planar) to truncated dipolar cases, going through the Heisenberg (isotropic) interaction. In Sec. III B we analyze the results obtained. First, we consider the transition from the short-time quadratic decay to the exponential regime in analogy to what is known for the SP. Then we focus on the exponential regime to show that the FGR in the present spin problem has independent contributions arising from each specific process in the $\mathcal{S}$-$\mathcal{E}$ interaction. We then compare these rates with a previous evaluation based on the contrast of specific interferences (ME attenuation). In the last section, we conclude that since the LE filters the internal dynamics of the system, it provides reliable and continuous access to all time regimes. Thus, the LE compares favorably with the evaluation of decoherence based on interference contrast.

II. QUANTUM DYNAMICS IN SPIN SYSTEMS

A. The models

The spin models analyzed in this article are schematized in Fig. 1. In the first one, the system $\mathcal{S}$ is an m-spin chain [Fig. 1(a)], which could constitute a quantum channel. It interacts with a second chain $\mathcal{E}$, which stands for the "environment" that perturbs the dynamics of $\mathcal{S}$. The second model [Fig. 1(b)] is obtained from the first one by imposing a periodic boundary condition that transforms chains into rings.

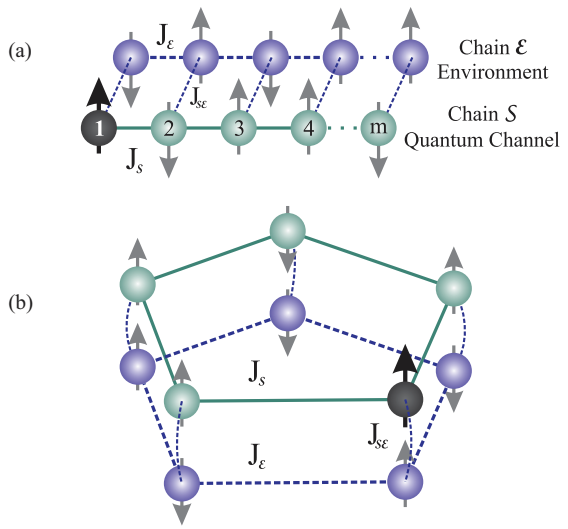

FIG. 1. (Color online) The spin system. (a) Open boundary conditions. (b) Closed boundary conditions (ring-like). Continuous (green) connections represent interactions that can be inverted to obtain the Loschmidt echo. Dash (blue) lines represent non-controllable interactions. The first spin (black circle) is initially polarized and the rest of the spins are in one of the high temperature configurations.

For both models, the spin Hamiltonian is given by

$$\hat{H}_{\text{total}} = \hat{H}_{\mathcal{S}} \otimes \hat{I}_{\mathcal{E}} + \hat{I}_{\mathcal{S}} \otimes \hat{H}_{\mathcal{E}} + \hat{V}_{\mathcal{SE}}, \tag{1}$$

where the first and second terms represent the system and the environment Hamiltonians, respectively, and the third one is the interaction between them. In order to simplify the notation, we write just $\hat{H}_{\mathcal{S}}$ and $\hat{H}_{\mathcal{E}}$ instead of the tensor product with their respective $\hat{I}_{\mathcal{E}}$ and $\hat{I}_{\mathcal{S}}$ identities. For both $\nu = \mathcal{S}$ and $\nu = \mathcal{E}$, we use an effective "planar" or XY Hamiltonian [18], which describes the homogeneous flip-flop interaction between nearest neighbor spins. In the model in Fig. 1(a), i.e., the chain,

$$\begin{aligned}\hat{H}_{\nu} &= \sum_{n=1}^{m-1} J_{\nu}\left(\hat{S}^{x}_{\nu,n+1}\hat{S}^{x}_{\nu,n} + \hat{S}^{y}_{\nu,n+1}\hat{S}^{y}_{\nu,n}\right) \\ &= \sum_{n=1}^{m-1} \frac{J_{\nu}}{2}(\hat{S}^{+}_{\nu,n+1}\hat{S}^{-}_{\nu,n} + \hat{S}^{-}_{\nu,n+1}\hat{S}^{+}_{\nu,n}).\end{aligned} \tag{2}$$

Here $\hat{S}^{x}_{\nu,n}$ and $\hat{S}^{y}_{\nu,n}$ are the x and y components of the spin operator at the nth site in the ν chain respectively, while $\hat{S}^{+}_{\nu,n}$ and $\hat{S}^{-}_{\nu,n}$ are the raising and lowering operators. Again, the abbreviated notation for any spin operator must be understood in the form $\hat{S}^{z}_{\mathcal{S},n} = \hat{I}_1 \otimes \cdots \otimes \hat{S}^{z}_{n} \otimes \cdots \otimes \hat{I}_m \otimes \hat{I}_{m+1} \otimes \cdots \otimes \hat{I}_{2m}$. If one wants to consider the ring model, an extra XY coupling appears between the first and the nth spins.

The interchain coupling is

$$\hat{V}_{\mathcal{SE}} = \sum_{n=1}^{m} J_{\mathcal{SE}}\left[2\alpha\hat{S}^{z}_{\mathcal{S},n}\hat{S}^{z}_{\mathcal{E},n} - \left(\hat{S}^{x}_{\mathcal{S},n}\hat{S}^{x}_{\mathcal{E},n} + \hat{S}^{y}_{\mathcal{S},n}\hat{S}^{y}_{\mathcal{E},n}\right)\right] \tag{3}$$

$$= \sum_{n=1}^{m} J_{\mathcal{SE}}\left[2\alpha\hat{S}^{z}_{\mathcal{S},n}\hat{S}^{z}_{\mathcal{E},n} - \frac{1}{2}(\hat{S}^{+}_{\mathcal{S},n}\hat{S}^{-}_{\mathcal{E},n} + \hat{S}^{-}_{\mathcal{S},n}\hat{S}^{+}_{\mathcal{E},n})\right], \tag{4}$$

where the first term is an Ising interaction. The α parameter determines the anisotropy of the coupling. This encompass the typical magnetic resonance scenarios: the XY (planar) interaction [18], represented by $\alpha = 0$; the Heisenberg (isotropic) interaction [39], by $\alpha = -\frac{1}{2}$; and the truncated dipolar coupling [40], corresponding to $\alpha = 1$. In order to extend and systematize our analysis we also consider several other values for α. It is important to note that for any finite α the $\mathcal{S}$-$\mathcal{E}$ interaction always has an XY component. This allows a polarization exchange which, in a Fermionic representation, can be seen as "single-particle tunneling" [41]. In such a picture, the Ising term corresponds to a nearest-neighbor Hubbard term which is a two-body interaction.

It is crucial to stress that the real constants $J_{\mathcal{S}}$, $J_{\mathcal{E}}$, and $J_{\mathcal{SE}}$ determine the relevant time scales of the whole dynamics. As introduced above, the first two give the homogeneous XY coupling within $\mathcal{S}$ and $\mathcal{E}$, respectively, while $J_{\mathcal{SE}}$ stands for the interchain coupling. To ensure smooth degradation of the $\mathcal{S}$ coherent dynamics, we set $J_{\mathcal{SE}}$ in the weak coupling limit, i.e., $J_{\mathcal{SE}} \ll J_{\mathcal{S}} = J_{\mathcal{E}}$.

B. Basic features of spin dynamics

A natural question for the spin models introduced above is how to quantify the decoherence of $\mathcal{S}$ in the presence of $\mathcal{E}$. This means that one has to deal with a composite (bipartite) Hilbert space $\mathcal{S}\otimes\mathcal{E}$ and trace out the $\mathcal{E}$ degrees of freedom whenever necessary. A standard strategy relies on finding an appropriate decoherence rate $1/\tau_\phi$ through the quantification of the attenuation of system's specific interferences. As in experiments [29,40], one starts evaluating the evolution of an injected local polarization through the spin autocorrelation function [39,42]:

$$P_{1,1}(t)=\frac{\langle\Psi_{\rm eq}|\hat{S}^z_{\mathcal{S},1}(t)\hat{S}^z_{\mathcal{S},1}(0)|\Psi_{\rm eq}\rangle}{\langle\Psi_{\rm eq}|\hat{S}^z_{\mathcal{S},1}(0)\hat{S}^z_{\mathcal{S},1}(0)|\Psi_{\rm eq}\rangle}. \tag{5}$$

This function gives the local polarization at time t along the z direction in site 1 provided that at time $t=0$ the system was in its thermal equilibrium state plus a local excitation at site 1. Here, the spin operator in the Heisenberg representation is given by $\hat{S}^z_{\mathcal{S},1}(t)=e^{i\hat{H}_{\rm total}t/\hbar}\hat{S}^z_{\mathcal{S},1}e^{-i\hat{H}_{\rm total}t/\hbar}$. The many-body state $|\Psi_{\rm eq}\rangle$ corresponding to a high-temperature thermal equilibrium represents a mixture of all states with amplitudes satisfying the appropriate statistical weights and random phases. Then the initial nonequilibrium local excitation $|\Psi_{\rm ne}\rangle$ can be defined in terms of the computational (Ising) basis components, which have the first spin up as

$$|\Psi_{\rm ne}\rangle=\frac{\hat{S}^+_{\mathcal{S},1}|\Psi_{\rm eq}\rangle}{|\langle\Psi_{\rm eq}|\hat{S}^-_{\mathcal{S},1}\hat{S}^+_{\mathcal{S},1}|\Psi_{\rm eq}\rangle|^{1/2}}=\sum_r c_r|\Psi_r\rangle; \tag{6}$$

see Appendix A for further details. Here, each contribution $|\Psi_r\rangle$ to the locally polarized initial state can be written as

$$|\Psi_r\rangle=|\uparrow_1\rangle\otimes|\beta_r\rangle, \tag{7}$$

where the basis for the remaining $2m-1$ spins is

$$\begin{aligned}&|\beta_r\rangle=|s_2\rangle\otimes|s_3\rangle\otimes|s_4\rangle\otimes\cdots\otimes|s_{2m}\rangle \quad \text{with}\\ &|s_k\rangle\in\{|\uparrow\rangle,|\downarrow\rangle\}.\end{aligned} \tag{8}$$

Since in the regime of NMR spin dynamics, the thermal energy k_BT is much higher than any other energy scale of the system [42,43], all statistical weights turn out to be identical, i.e., $|c_r|=1/\sqrt{2^{2m-1}}$.

It is useful to analyze the autocorrelation $P_{1,1}(t)$. For each contribution $|\Psi_r\rangle$ to the initial state, the evolved wave function at time t is

$$|\Psi_r(t)\rangle=\exp\left\{-\frac{\rm i}{\hbar}\hat{H}_{\rm total}t\right\}|\Psi_r\rangle. \tag{9}$$

Then the probability of finding the first spin up-polarized is

$$P^{[r]}_{1,1}(t)=\sum_j|(\langle\uparrow_1|\otimes\langle\beta_j|)|\Psi_r(t)\rangle|^2, \tag{10}$$

where the sum runs over the 2^{2m-1} configurations of the $2m-1$ remaining spins. Note that the sum over the j index in Eq. (10) means that we are performing a trace not only over $\mathcal{E}$, but also over the spins in $\mathcal{S}$ other than the first one. After the summation over all contributions $|\Psi_r\rangle$ to the initial state, and expressing the result as a local polarization [28], we obtain

$$P_{1,1}(t)=\left[\sum_{r=1}^{2^{2m-1}}|c_r|^2\,P^{[r]}_{1,1}(t)-\frac{1}{2}\right]\times 2. \tag{11}$$

A computation of the time-dependent local observable in Eq. (5) reduces to Eq. (11), which, in turn, requires evolving each of the 2^{2m-1} pure states to evaluate the ensemble-averaged observables. This is implemented using a Trotter decomposition [44] assisted by an algorithm that exploits quantum parallelism [45] (see Appendix B).

C. The single-particle picture and mesoscopic echoes

The obvious complexity of many-spin dynamics might hinder some simple interference phenomena that can be taken as hallmarks. Under certain experimentally achievable conditions (e.g., XY interaction, 1D topology, and negligible $\mathcal{S}$-$\mathcal{E}$ interaction), the autocorrelation $P_{1,1}(t)$ becomes a simple one-body magnitude. Indeed, once the initial excitation is created, the first physical picture about its evolution may be obtained from the Wigner-Jordan spin-fermion mapping [46]. The point here is to trace over the $\mathcal{E}$ degrees of freedom from the beginning and focus on a single-quantum spin chain. Accordingly, an isolated m spin chain with XY interaction, where N of them are up, is mapped to a chain with N noninteracting fermions. Thus, a local polarization excitation has the same dynamics as a single-fermion wave packet in a tight-binding linear chain [41,47]. The observed autocorrelation function in the limit of infinite temperature is precisely described by the evolution of a single spin up in a chain of down spins:

$$|\Psi_1\rangle:=|\uparrow_1\rangle\otimes|\downarrow_2\rangle\otimes|\downarrow_3\rangle\otimes\cdots\otimes|\downarrow_m\rangle\,. \tag{12}$$

This is a one-body wave function, defined on a subspace of $\mathcal{S}$ where the total spin projection is $\frac{m}{2}-1$, and the observable is evaluated as

$$P^{[r=1]}_{1,1}(t)=|\langle\Psi_1|\exp[-i\hat{H}_{\mathcal{S}}t/\hbar]|\Psi_1\rangle|^2. \tag{13}$$

Since this is a finite-size system one should expect revivals of the initial polarization. Such revivals are called MEs [28,30] and they appear when constructive interferences manifest at the Heisenberg time $t_H\sim\hbar/\Delta$, with Δ being the typical mean energy level spacing. In a spin chain with XY interaction one may safely use $\Delta\simeq J_{\mathcal{E}}/m$. As long as this one-body picture remains approximately valid for a linear chain weakly coupled to the environment, these interferences show up experimentally [18,29,48].

A weak coupling to the spin bath $\mathcal{E}$ results in progressive attenuation of the ME, which has been used to quantify environmentally induced decoherence [31]. This attenuation is understood as an FGR, which describes an "irreversible" decay of a pure state in $\mathcal{S}$ into collective $\mathcal{S}\otimes\mathcal{E}$ states. In fact, the validity of the FGR here requires the breakdown of degeneracies, i.e., the whole $\mathcal{S}\otimes\mathcal{E}$ must behave as a fully many-body system. We return to this point below.

D. The Loschmidt echo

Let us now explain the essence of the protocol that uses the LE to quantify decoherence in a spin system using a local spin as an observable [7]. Our strategy relies on the controllability of chain $\mathcal{S}$, whose Hamiltonian's sign can be switched at will as is often the case in NMR. The reversibility of the dynamics within the chain is perturbed by the interaction with the noncontrolled spin chain $\mathcal{E}$. There are two stages in the evolution. First, a spin excitation is created and the whole spin set evolves according to the Hamiltonian, Eq. (1), during a time t_R. At that time, the internal interactions within $\mathcal{S}$ are reversed (i.e., $\hat{H}_{\mathcal{S}}$ is replaced by $-\hat{H}_{\mathcal{S}}$ during a second t_R period). However, neither the $\mathcal{S}$-$\mathcal{E}$ coupling nor the interactions within chain $\mathcal{E}$ are reversed, leading to a nonreversed perturbation,

$$\hat{\Sigma} = \hat{H}_{\mathcal{E}} + \hat{V}_{\mathcal{SE}}, \tag{14}$$

acting in *both* periods. Thus, in analogy with Eq. (5), we define the observable LE as the recovered local polarization:

$$M_{\mathrm{LE}}(2t_R) = \frac{\langle \Psi_{\mathrm{eq}} | \hat{S}^z_{\mathcal{S},1}(2t_R)\hat{S}^z_{\mathcal{S},1}(0) | \Psi_{\mathrm{eq}} \rangle}{\langle \Psi_{\mathrm{eq}} | \hat{S}^z_{\mathcal{S},1}(0)\hat{S}^z_{\mathcal{S},1}(0) | \Psi_{\mathrm{eq}} \rangle}. \tag{15}$$

The spin operators, expressed in the Heisenberg representation, are now

$$\hat{S}^z_{\nu,1}(2t_R) = e^{\frac{i}{\hbar}(-\hat{H}_{\mathcal{S}}+\hat{\Sigma})t_R} e^{\frac{i}{\hbar}(\hat{H}_{\mathcal{S}}+\hat{\Sigma})t_R} \hat{S}^z_{\nu,1} e^{-\frac{i}{\hbar}(\hat{H}_{\mathcal{S}}+\hat{\Sigma})t_R} \times e^{-\frac{i}{\hbar}(-\hat{H}_{\mathcal{S}}+\hat{\Sigma})t_R}. \tag{16}$$

The computation of the LE in Eq. (15) proceeds as above for the forward dynamics. In a system with a general interaction, it requires a full many-body evolution.

As before, the initial excitation is described in terms of the Ising basis by Eq. (6). For each contribution $|\Psi_r\rangle$ to the initial state, the resulting wave function at time $t = 2t_R$, after the whole time-reversal procedure, is

$$|\Psi_r(2t_R)\rangle = \exp\left\{-\frac{i}{\hbar}(-\hat{H}_{\mathcal{S}} + \hat{\Sigma})t_R\right\} \times \exp\left\{-\frac{i}{\hbar}(\hat{H}_{\mathcal{S}} + \hat{\Sigma})t_R\right\} |\Psi_r\rangle\,. \tag{17}$$

In analogy with the discussion above, the probability of finding the first spin up-polarized is

$$M^{[r]}_{1,1}(t) = \sum_j |(\langle\uparrow_1| \otimes \langle\beta_j|)|\Psi_r(t)\rangle|^2, \tag{18}$$

where the sum runs over the 2^{2m-1} configurations of the $2m-1$ remaining spins. Again, the sum over j means a trace over all the spins of the environment and the system except the first one. After the summation (average) over all contributions $|\Psi_r\rangle$ to the initial state, and expressing the result as a local polarization, we compute the local LE as

$$M_{\mathrm{LE}}(t) = \left[\sum_{r=1}^{2^{2m-1}} |c_r|^2\, M^{[r]}_{1,1}(t) - \frac{1}{2}\right] \times 2. \tag{19}$$

Here again, the statistical weights $|c_r|^2$ are the inverse of 2^{2m-1}, the number of initial states in the ensemble that satisfy the "*first spin up-polarized*" condition. Note that, except for the fact that the evolution operator contains a partially reversed dynamics, this quantity refers to the same physical observable as Eq. (11).

E. Connection to previous works

It would be useful to make a connection between the observable just described and the usual definition of the LE [32], which was extensively studied in the field of quantum chaos and quantum information [36,37]. With this purpose, let us consider the particular case in Fig. 1, where $\hat{H}_{\mathcal{S}}$ describes a chain with XY interactions, while $\hat{H}_{\mathcal{E}}$ describes a chain $\mathcal{E}$ that remains quenched in a random configuration and $\hat{V}_{\mathcal{SE}}$ is restricted to an Ising interaction. Under these assumptions, the time-reversed dynamics reduces to that of a single spin up in an oriented chain defined in Eq. (12). Accordingly, $\hat{\Sigma}$ becomes an Hermitian self-energy operator $\hat{\Sigma}_{\mathcal{S}}$ acting on the $\mathcal{S}$ Hilbert space. Indeed, $\hat{\Sigma}_{\mathcal{S}}$ represents a set of nonreversed random energy shifts produced by the Ising interaction with static environmental spins. In the independent fermion picture, $\hat{\Sigma}_{\mathcal{S}}$ yields a "random potential" for each specific configuration of the environment, i.e., the binary alloy variant of Anderson's disorder [49]. It is now relevant to address the physical meaning of the sum over the 2^{2m-1} indices r of the observable in Eq. (19). This sum performs a trace over system spins which evolve but are not observed (crucial to recovery of a one-body dynamics), as well as a trace over the environmental spins, which can be seen as an ensemble average over quenched disorder configurations [32]. Thus, the same procedure that enabled us to reduce Eqs. (5) to (13) transforms Eq. (15) into the corresponding one-body LE:

$$M_{\mathrm{LE}}(2t_R) = \left| \langle\Psi_1| \exp\left\{-\frac{i}{\hbar}(-\hat{H}_{\mathcal{S}} + \hat{\Sigma}_{\mathcal{S}})t_R\right\} \times \exp\left\{-\frac{i}{\hbar}(\hat{H}_{\mathcal{S}} + \hat{\Sigma}_{\mathcal{S}})t_R\right\} |\Psi_1\rangle \right|^2. \tag{20}$$

Here, one can recognize the LE definition introduced in Ref. [32] as the overlap of two wave functions evolving in the presence of a quenched disorder whose dynamics is not inverted.

The decomposition of the spin set into a controllable subset ($\mathcal{S}$) and an uncontrollable one ($\mathcal{E}$) resembles the discussion of the partial fidelity, called the Boltzmann echo, analyzed in Ref. [50] for a two-body problem. Analogously, the $2m$ spin problem treated here verifies that (i) separation into two interacting subsystems ($\mathcal{S}$ and $\mathcal{E}$) is performed; (ii) the initial state in $\mathcal{S}$ is at least partially prepared (injected polarization), and at the end a local measure is performed at the same site of injection; (iii) the subsystem $\mathcal{E}$ remains in the high-temperature thermal equilibrium; and (iv) the Hamiltonian in $\mathcal{S}$ can be fully time reversed, while the Hamiltonian of $\mathcal{E}$ and the $\mathcal{S}$-$\mathcal{E}$ interaction remain uncontrolled. However, the main result of Ref. [50], which considers a *chaotic* one-body system coupled to a *chaotic* one-body environment, cannot be directly compared with our study. Here, we focus on a system and an environment which are both many-body systems that can be reduced to *integrable* one-body systems. In our case, we expect many-body chaos [51] only as a consequence of the $\mathcal{S}$-$\mathcal{E}$ interaction.

Many-body chaos has been the subject of much interest [52–54] and was recently renewed mainly in connection with thermalization dynamics [55]. Within this context, the attention has been centered on the study of spectral correlations and the related SP, i.e., the decay of an initial excitation [38]. Based on general considerations on the strength function or local density of states [56], one may predict a Gaussian (or quadratic) time decay governed by the second moment of the perturbation σ^2, followed by an exponential regime whose rate is described by the FGR:

$$1/\tau_{\rm FGR} = \frac{2\Gamma}{\hbar} = \frac{2\pi}{\hbar}\sigma^2 N_1. \tag{21}$$

Here, N_1 is the density of directly connected states (DDCS). While it might seem elusive, this magnitude can be numerically evaluated with a Lanczos algorithm [57]. It also accounts for the transition time from the short-time quadratic regime to the exponential one. Accordingly, the crossover to the exponential regime is expected [38,58] to occur at $t_s \simeq (\tau_{\rm FGR}\sigma^2)^{-1} = (2\pi/\hbar)N_1$. This *spreading time* characterizes the dissemination of an excitation within the environment. In the many-body context, an interpolation formula has been proposed [38],

$$P_{11}(t) = \exp\left[2\frac{\Gamma^2}{\sigma^2} - 2\sqrt{\frac{\Gamma^4}{\sigma^4} - \Gamma^2 t^2/\hbar^2}\right], \tag{22}$$

which, to our knowledge, has not been checked in concrete systems.

Coming back to our model, when chain $\mathcal{S}$ is isolated, the localized excitation propagates freely, and the LE will have a constant value of 1. However, once a weak $\hat{V}_{\mathcal{SE}}$ interaction is turned on, the excitation decays into the chain $\mathcal{E}$ and the local LE degrades progressively with a law that would be closely described as a SP. Thus, for long chains where the spectrum is a quasicontinuum, we expect that the short and intermediate time regimes of the LE would follow closely the above discussion for the SP. In fact, we analyze the LE decay numerically and study the rates testing the validity of an FGR description [59]. When applied to the present many-body context, it would be

$$\frac{1}{\tau_\phi} \simeq \sum_\delta \frac{2\pi}{\hbar}\left|V^\delta_{\mathcal{SE}}\right|^2 N_{1\delta}, \tag{23}$$

where $|V^\delta_{\mathcal{SE}}|^2 \equiv \sigma^2$ is the local second moment of the process δ (e.g., Ising or XY) contributing to the $\mathcal{S}$-$\mathcal{E}$ interaction and $N_{1\delta}$ represents some appropriate DDCS.

III. QUANTIFYING DECOHERENCE THROUGH THE LOSCHMIDT ECHO

A. Numerical results in spin chains

In this section we present the results obtained for $M_{\rm LE}(t)$ in the spin models represented in Fig. 1. Even though our major concern is the exponential decay described by the FGR, we can also identify the short-time quadratic decay and the saturation regime, as shown in Fig. 2. It is noticeable that the LE yields results for a very wide range of parameters and time scales. This feature contrasts with the study of interferences through the ME, whose observability restricts the quantification of decoherence.

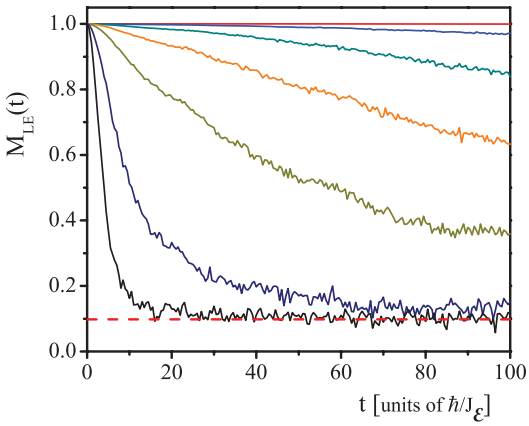

FIG. 2. (Color online) Time regimes of the local Loschmidt echo. Numerical results for a ring of five spins weakly coupled to another identical ring by an XY interchain interaction ($\alpha = 0$). The $M_{\rm LE}$ is plotted as a function of the total evolution time $t = 2t_R$. Note that the stronger the interchain coupling $J_{\mathcal{SE}}$, the faster the saturation regime is reached (dashed line). From top to bottom, the different curves correspond to the coupling parameters $J_{\mathcal{SE}}$—0.001, 0.01, 0.025, 0.05, 0.1,0.25, and 0.5—in units of $J_{\mathcal{E}}$.

In Fig. 3(a) the short-time dynamics is compared with the expected quadratic decay (dotted line), which should appear in any quantum evolution at short times. Indeed,the plot of $(1 - M_{\rm LE})/J^2_{\mathcal{SE}}$ (on a log-log scale) as a function of time shows that $M_{\rm LE}$ follows a quadratic function:

$$M_{\rm LE}(t) \simeq 1 - \left[\frac{J_{\mathcal{SE}}}{2\hbar}\right]^2 t^2. \tag{24}$$

This confirms that the short-time decay is determined by $\sigma^2 = (J_{\mathcal{SE}}/2\hbar)^2$, the second moment of the $\mathcal{SE}$ interaction. The agreement is observed until a time $t_s \simeq \hbar/J_{\mathcal{E}}$, which verifies the prediction for t_s in terms of the $\mathcal{E}$ dynamics. For comparison, we show in Fig. 3(b) the SP of an excitation in a single-spin system $\mathcal{S}$ that interacts with the edge of a spin chain $\mathcal{E}$ where it can spread through pure XY interactions. This model, shown in the inset, constitutes a paradigm for the onset of the FGR, because the DDCS is precisely defined by $N_1 = 1/J_{\mathcal{E}}$ and remains independent of $J_{\mathcal{SE}}$ [60]. In Fig. 3(b), we also show by the dashed line the interpolative expression in Eq. (22) for the strongest coupling. The latter expression deviates more rapidly from the quadratic decay than the SP in the one-body chain.

The onset of the exponential regime is exemplified in Fig. 4 for a few values of a pure $XY\mathcal{SE}$ interaction. As a general tendency, we observe that the asymptotic exponential decay becomes well defined only after some evolution period. We indicate by an arrow the initial data that we use to fit these rates. For comparison, the SP interpolative expression is plotted for the same decay rates. We note that for $J_{\mathcal{SE}}/J_{\mathcal{E}} \lesssim 0.085$ the interpolation starts to lie below the numerical results, and longer times are required to define the asymptotic exponential.

For long times, the LE shows a saturation plateau at $1/10$ (see Fig. 2). This observation is consistent with the expectation that, within these coupling networks, the finite system of interacting spins behaves ergodically under LE dynamics, and thus the polarization spreads uniformly. At long times each

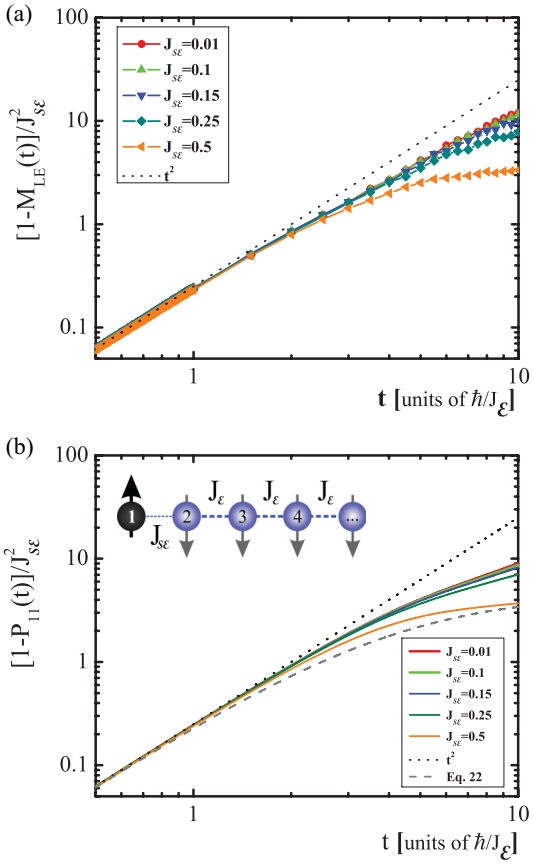

FIG. 3. (Color online) (a) Short-time behavior of the Loschmidt echo. The dotted line is the quadratic decay [Eq. (24)]. (b) Short-time behavior of the survival probability for an XY spin chain described by $\hat{H}_{\rm total} = J_{S\mathcal{E}}(\hat{S}_1^+\hat{S}_2^- + \hat{S}_2^+\hat{S}_1^-) + J_{\mathcal{E}}\sum_{n=2}^{\infty}(\hat{S}_n^+\hat{S}_{n+1}^- + \hat{S}_{n+1}^+\hat{S}_n^-)$, where the first spin is the system and the others constitute the environment. This system is known to satisfy the FGR [60]. Note the similarity between (a) and (b) in departing from the quadratic decay, which evinces the spreading time t_s. The dashed line shows a plot of Eq. (22) for $J_{S\mathcal{E}} = 0.5J_{\mathcal{E}}$.

site is polarized by the amount $1/(2m)$. The larger the coupling $J_{S\mathcal{E}}$, the more rapidly the asymptotic saturation is reached.

In order to assess the exponential regime, we plot the characteristic rate $1/\tau_\phi$ in Fig. 5(a) as a function of $J^2_{S\mathcal{E}}$ in units of $J_{\mathcal{E}}/\hbar$. This quantity is appropriate to verify the FGR [Eq. (23)], as long as $J^2_{S\mathcal{E}}$ is the typical scale for the second moment of the $\mathcal{S}$-$\mathcal{E}$ interaction and $1/J_{\mathcal{E}}$ that of N_1, the DDCS. We point out that rate calculations with longer rings and chains are seen to give similar values as long as the above parameters are kept the same. Such independence of m resembles the SP and LE for a single spin interacting with chains of different lengths [60,61]. This is indicative that we are reaching the limit where the DDCS becomes dense enough to manifest the sum rule intrinsic to the FGR [57]. Thus, we restrict our analysis to cases with $m = 5$. Although several forms of the interchain Hamiltonians were considered by varying the anisotropy parameter α, we show only those relevant to NMR experiments: XY ($\alpha = 0$), isotropic ($\alpha = -\frac{1}{2}$), and truncated dipolar interaction ($\alpha = 1$). We observe that the boundary conditions play a nontrivial role [41]. For the case of open boundary conditions [Fig. 1(a)], some oscillations appear

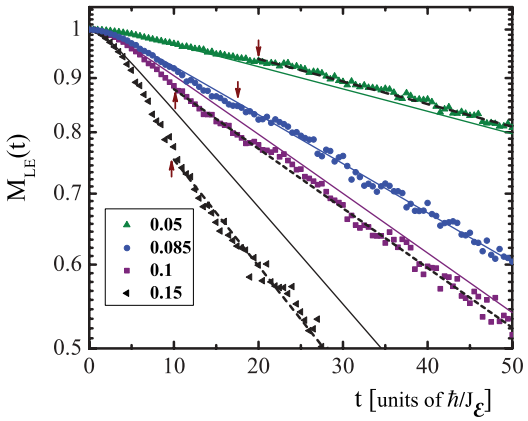

FIG. 4. (Color online) Onset of the LE exponential decay. On the log scale, the dashed lines are the ideal exponentials determined by the fitting, shown here for representative values. The delay in the entrance into the exponential regime is indicated by arrows pointing to the first data used in the fitting. Solid lines represent the interpolative Eq. (22), used with the corresponding σ^2 and Γ.

mounted on a decay which also depends on the parity of m, the number of spins in each chain. Here, we present only the results using closed boundary conditions (rings), where these effects are much weaker.

Note that the LE allows one to explore a range of very weak perturbations yielding τ_ϕ from the regime of exponential decay. This range was inaccessible in the interference contrast method [31]. We observe that the rates in Fig. 5(a) start from 0 and show a rapid increase with the $J_{S\mathcal{E}}$ perturbation. After a small perturbation threshold the rates slow down to a linear dependence on the second moment of the perturbation. This confirms the validity of Eq. (23) for this range. The linear fit is shifted by an offset, $1/\tau_0$, which seems to depend on the nature of the $S\mathcal{E}$ interaction, as it becomes larger for perturbations with bigger Ising components.

Figure 5(b) shows the FGR contribution to the scaled decoherence rates $[1/\tau_\phi - 1/\tau_0]/J^2_{S\mathcal{E}}$ as a function of interaction anisotropy α^2. There we also include the rates derived from the ME attenuation [31]. From the slope in that plot we derive the contributions to the global decay rate $1/\tau_\phi$, arising from XY and Ising processes in the interchain interaction:

$$\frac{1}{\tau_\phi} = \frac{1}{\tau_0} + \frac{1}{\tau_\phi^{XY}} + \frac{1}{\tau_\phi^{ZZ}}. \tag{25}$$

For LE results

$$\text{LE}: \frac{1}{\tau_\phi^{XY}} = (0.92 \pm 0.04)\frac{J^2_{S\mathcal{E}}}{\hbar J_{\mathcal{E}}}, \tag{26}$$

$$\text{LE}: \frac{1}{\tau_\phi^{ZZ}} = (1.12 \pm 0.04)\alpha^2\frac{J^2_{S\mathcal{E}}}{\hbar J_{\mathcal{E}}}. \tag{27}$$

In order to compare with the numerical results in Ref. [31], and translating its notation $-a/b \equiv 2\alpha$, the rates contributing to the ME degradation result:

$$\text{ME}: \frac{1}{\tau_\phi^{XY}} = (1.00 \pm 0.06)\frac{J^2_{S\mathcal{E}}}{\hbar J_{\mathcal{E}}}, \tag{28}$$

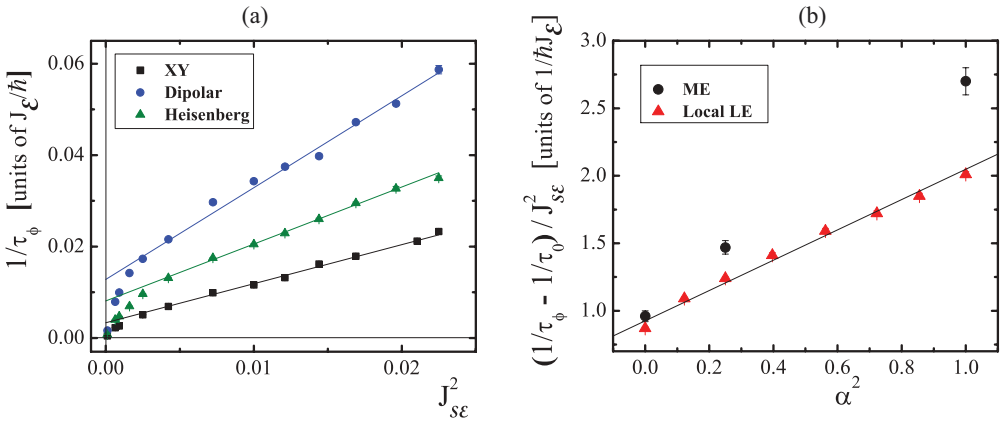

FIG. 5. (Color online) (a) Decay rates for NMR-relevant interchain couplings, in units of $J_\mathcal{E}/\hbar$. The slopes and offsets depend on the value of α, i.e., on the relative weight between the Ising (dephasing) and the XY (polarization transfer) contributions to the interchain coupling. (b) Scaled rates showing the additivity of the $XY$and Ising contributions to the FGR rate as a function of α^2. For comparison, the rates obtained from mesoscopic echo (ME) degradation data obtained in Ref. [31] are also plotted.

$$\text{ME}: \frac{1}{\tau_\phi^{ZZ}} = (2.0 \pm 0.3)\alpha^2 \frac{J^2_{\mathcal{SE}}}{\hbar J_\mathcal{E}}. \tag{29}$$

The most striking effect evinced by this comparison is that while the XY contributions are essentially the same in both methods, the Ising contribution (i.e., pure dephasing) in the ME [Eq. (29)] is almost twice the value obtained from the local LE. In the following section we analyze the origin of this result.

B. Analysis of decoherence regimes

First, we address the applicability of an "*SP picture*" for the LE in the present case, as proposed in Sec. II in connection with previous works. We verified that the short-time decay is naturally ruled by the second moment of the $\mathcal{S}$-$\mathcal{E}$ interaction $\sigma^2 = [J_{\mathcal{SE}}/2]^2$. We also checked the estimation for the spreading time $t_s \simeq \hbar/J_\mathcal{E}$, i.e., the transition from the quadratic short-time to the exponential regime. We found that this prediction is in agreement with the observed end of the quadratic decay.

In our spin problem, the LE exponential regime needs a further delay beyond t_s to become well defined. This indicates that the DDCS is not immediately defined but $J_{\mathcal{SE}}$ may have a role in its stabilization. Indeed, a back action of $J_{\mathcal{SE}}$ is needed to break the strong degeneracy present in the unperturbed integrable $\mathcal{E}$, a finite XY chain itself. Only then, one has the sufficiently dense spectrum required for the FGR to apply. Once the whole Hilbert space is made accessible by the perturbation, as many as $\binom{2m}{m}$ states become coupled by an interaction that conserves spin projection.

The interpolative Eq. (22) approximates satisfactorily the short-time decay, but it is not as well suited for intermediate times and certainly cannot be applied to the saturation regime. These deviations can, in principle, be related to a failure in the SP picture to describe the local LE dynamics. The physics underlying Eq. (22) is based on the assumption of a sufficiently large number of particles and a well-defined N_1. Also, one should be aware that our spin case is strictly finite, indeed quite small, and therefore the polarization cannot relax to 0. The observed asymptotic steady magnetization $1/2m$ can be identified with an ergodic behavior of the excitation described by the local LE dynamics. Since this ergodicity is not present in the unperturbed system, it should emerge as a consequence of the $\mathcal{SE}$ interaction.

It is important to note that neither the rate obtained nor σ^2 depends on the total number of spins or on the number of spins in $\mathcal{S}$. The reason for such independence is related to the initial nonequilibrium condition stated in Eq. (6), which is a well-localized excitation that maintains its character when it propagates through an XY chain. It turns out that such localized excitation behaves much like a single particle and, in some sense, almost classically. This remains true at least when the LE is in the exponential regime. We have seen that the independence of the number of spins does not hold if one considers an initial state built in as an arbitrary superposition. However, investigation of this issue goes beyond the scope of the present study.

One should note that splitting the FGR contribution to the decoherence rate into two well-separated terms, a strategy also exploited in Ref. [31], demonstrates the additivity of the XY and Ising processes. Each of them is associated with a different term in the interaction coupling $\hat{V}_{\mathcal{SE}}$ and requires a different DDCS. These properties are indeed manifested in Fig. 5, which shows the linear dependence of $(1/\tau_\phi - 1/\tau_0)/J^2_{\mathcal{SE}}$ on the relative weight α^2.

Comparing the rates obtained through the LE with those computed by the ME degradation [31], we note that the XY rates are equivalent and we can interpret such equivalence by using the mapping into a one-body evolution in both $\mathcal{S}$ and $\mathcal{E}$. Even when the one-body picture is not rigorously valid when the interaction $\hat{V}_{\mathcal{SE}}$ is turned on, it provides some physical insights [61] that apply to more complex cases. Accordingly, the dynamics along the chains is only weakly affected by the tunneling processes (i.e., in a single-particle picture, the kinetic energy along the chains commutes with that along the interchain direction). Thus, the rate $1/\tau_\phi^{XY}$ should coincide with the interchain tunneling rate, and we expect that it should not be affected by a time-reversal procedure within $\mathcal{S}$.

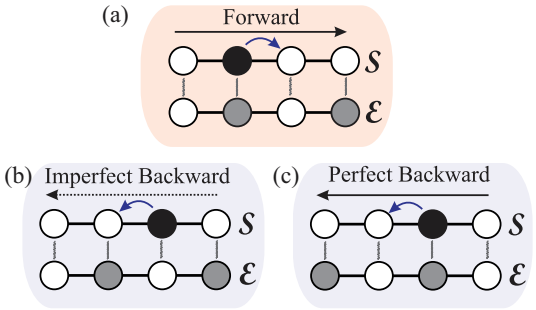

FIG. 6. (Color online) Spin propagation in the presence of an Ising interchain interaction, represented as a single fermion moving through a binary alloy landscape. A filled circle is a spin up or a fermion, and an open circle represents a spin down or a hole. All the processes are considered on the short time scale given by a single Trotter time step. (a) Forward dynamics within the upper chain $\mathcal{S}$, in the presence of the "random site energies" produced by the Ising interaction with the lower chain $\mathcal{E}$. (b) If $\mathcal{E}$ remains frozen, the backward evolution in $\mathcal{S}$ is imperfect because the signs of the "site energies" are not inverted. (c) A particular evolution of $\mathcal{E}$ provides a perfectly reversed dynamics for $\mathcal{S}$. In this case, the local portion of the potential landscape, which determined the excitation's forward evolution, is reversed.

In contrast to the simple decay associated with the XY component of the $\mathcal{S}$-$\mathcal{E}$ interaction, the Ising part causes energy fluctuations that induce a diffusion-like process within the system. This tends to blur out the dynamical recurrences (i.e., MEs). The lower decoherence rate observed from the LE indicates that the time reversal procedure is at least partially effective to reverse such processes. In fact, the rates for the pure Ising interaction observed here from the LE are about half those obtained from the ME [31]. This means that the ME attenuation overestimates the phase degradation induced by the environment. As stated before, the displacement of a spin excitation in the presence of a quenched spin environment plays the role of an Anderson disorder degrading the wave-packet dynamics that produces the ME. This degradation is computed as decoherence. The reversal of the internal XY interaction would not be able to reverse this disorder. However, if the environment has an inner dynamics on a time scale comparable to that of the system ($J_{\mathcal{S}} \simeq J_{\mathcal{E}}$), there are particular fluctuations that allow for a perfect reversal of the system dynamics. Indeed, this occurs when both the hopping and the site energy signs are inverted. Such specific $\mathcal{E}$ fluctuations are those needed to unravel the phase shifts produced during the forward evolution. This argument, which relies on a single-particle picture and equivalent time scales for the local dynamics in $\mathcal{S}$ and $\mathcal{E}$, is represented in Fig. 6. Thus, one may safely say that, in the presence of a fluctuating environment, the LE is able to reconstruct the phases in an appreciable fraction of the local configurations.

IV. CONCLUSIONS

We have presented an evaluation of decoherence for a spin chain in realistic many-body scenarios. As specific realizations for structured environments, we have used a second spin chain weakly coupled to the first. This system-environment interaction ranges from pure XY to truncated dipolar, passing through the isotropic Heisenberg interaction. In order to evaluate decoherence, we resorted to the LE, which here is the local polarization recovered after an imperfect time reversal procedure. The attenuation of such echoes yields a first-hand estimation of the decoherence rate, without any *ad hoc* assumptions about spectral functions [62,63] or stochastic noise operators [64,65]**.**Our computational technique involves a Trotter-Suzuki decomposition assisted by a recently developed algorithm that relies on quantum parallelism to evaluate local observables [45].

In the present many-body context, the decoherence rate is separated into two contributions, both of which scale with $J_{\mathcal{SE}}^2$ and $1/J_{\mathcal{E}}$, i.e., as an FGR. The rates obtained here do not depend on the number of spins m. This is strongly related to the localized initial condition, but this independence does not hold if the initial condition is a superposition state. It is also indicative of a specific sum rule relating the *local* second moment of the interaction and the DDCS, which in this many-body case coincides with that resulting from a single-particle picture.

In the adopted model, the close connection between the LE and the SP allows for a comparison with the expectancies of the last magnitude. In particular, we assessed an interpolative formula [38] that matches the initial quadratic decay with the exponential regime. Despite the qualitative agreement, the LE evidences a richer and more complex dynamical behavior than those predictions. For instance, the breakdown of single-particle degeneracies due to the $\mathcal{S}$-$\mathcal{E}$ interaction and the appearance of an ergodic regime, manifested as a steady saturation, are now clearly shown in the numerical results.

The numerical studies performed here confirm that the LE is better to quantify decoherence than the standard analysis based on interference degradation, as it recovers information that escapes such an analysis [31]. Additionally, by compensating the intrinsic dynamical interferences of the system through time reversal, the LE gets rid of most of the trivial part of the $\mathcal{S}$ dynamics that conceals the decoherence effects. Thus the LE provides smooth and continuous access to characterize decoherence processes.

ACKNOWLEDGMENTS

We acknowledge Fernando Pastawski for critical comments on the initial version of the manuscript, as well as Gonzalo Usaj and Greg Boutis for lively discussions. This work was performed with financial support from CONICET, ANPCyT, SeCyT-UNC, and MinCyT-Cor and an NVIDIA professor partnership program.

APPENDIX A: THE SPIN AUTOCORRELATION FUNCTION

We show here equivalent expressions for the spin autocorrelation expressed in Eq. (5). The autocorrelation $P_{1,1}(t)$ gives the local polarization at time t along the z direction at site 1, provided that at time $t = 0$ the system was in its thermal equilibrium state plus a local excitation in site 1. In order to show this assertion explicitly, we rewrite the numerator

in Eq. (5),

$$\langle\Psi_{\rm eq}|\hat{S}_1^z(t)\hat{S}_1^z(0)|\Psi_{\rm eq}\rangle = \langle\Psi_{\rm eq}|\left(\hat{S}_1^+(t)\hat{S}_1^-(t)-\tfrac{1}{2}\right)\left(\hat{S}_1^+(0)\hat{S}_1^-(0)-\tfrac{1}{2}\right)|\Psi_{\rm eq}\rangle, \quad \text{(A1)}$$

where we have used the identity $\hat{S}^z = \hat{S}^+\hat{S}^- - \frac{1}{2}$, which is valid for spins $1/2$. The $\mathcal{S}$ label has been dropped for simplicity. Then

$$\langle\Psi_{\rm eq}|\hat{S}_1^z(t)\hat{S}_1^z(0)|\Psi_{\rm eq}\rangle = \langle\Psi_{\rm eq}|\hat{S}_1^+(t)\hat{S}_1^-(t)\hat{S}_1^+(0)\hat{S}_1^-(0)|\Psi_{\rm eq}\rangle - \tfrac{1}{4}, \quad \text{(A2)}$$

where we have rearranged the terms and used the high-temperature hypothesis for $|\Psi_{\rm eq}\rangle$ explicitly, i.e., $\langle\Psi_{\rm eq}|\hat{S}_1^z(t)|\Psi_{\rm eq}\rangle = \langle\Psi_{\rm eq}|\hat{S}_1^z(0)|\Psi_{\rm eq}\rangle = 0$. It is crucial now to identify the meaning of the expectation value $\langle\Psi_{\rm eq}|\cdots|\Psi_{\rm eq}\rangle$ as a trace over the basis states (see Eq. (3) in Ref. [41]). Hence, the invariance of the trace under cyclic permutation leads to

$$\langle\Psi_{\rm eq}|\hat{S}_1^z(t)\hat{S}_1^z(0)|\Psi_{\rm eq}\rangle = \langle\Psi_{\rm eq}|\hat{S}_1^-(0)\hat{S}_1^+(t)\hat{S}_1^-(t)\hat{S}_1^+(0)|\Psi_{\rm eq}\rangle - \tfrac{1}{4}, \quad \text{(A3)}$$

and one identifies the nonequilibrium initial condition $\hat{S}_1^+(0)|\Psi_{\rm eq}\rangle$, which, after normalization, yields exactly Eq. (6):

$$|\Psi_{\rm ne}\rangle = \frac{\hat{S}_{\mathcal{S},1}^+|\Psi_{\rm eq}\rangle}{|\langle\Psi_{\rm eq}|\hat{S}_{\mathcal{S},1}^-\hat{S}_{\mathcal{S},1}^+|\Psi_{\rm eq}\rangle|^{1/2}}. \quad \text{(A4)}$$

Accordingly, the numerator can be written as

$$\begin{aligned}\langle\Psi_{\rm eq}|\hat{S}_1^z(t)\hat{S}_1^z(0)|\Psi_{\rm eq}\rangle &= |\langle\Psi_{\rm eq}|\hat{S}_{\mathcal{S},1}^-\hat{S}_{\mathcal{S},1}^+|\Psi_{\rm eq}\rangle|\langle\Psi_{\rm neq}|\hat{S}_1^+(t)\hat{S}_1^-(t)|\Psi_{\rm neq}\rangle - \tfrac{1}{4}\\ &= \tfrac{1}{2}\langle\Psi_{\rm ne}|\hat{S}_1^+(t)\hat{S}_1^-(t)|\Psi_{\rm ne}\rangle - \tfrac{1}{4}. \quad \text{(A5)}\end{aligned}$$

The denominator in Eq. (5) is $\langle\Psi_{\rm eq}|\hat{S}_1^z(0)\hat{S}_1^z(0)|\Psi_{\rm eq}\rangle \equiv \frac{1}{4}$. Therefore,

$$P_{1,1}(t) = 2\langle\Psi_{\rm ne}|\hat{S}_1^+(t)\hat{S}_1^-(t)|\Psi_{\rm ne}\rangle - 1. \quad \text{(A6)}$$

In the Schrödinger picture it yields

$$P_{1,1}(t) = 2\langle\Psi_{\rm ne}|e^{i\hat{H}_{\rm total}t/\hbar}\hat{S}_1^+\hat{S}_1^-e^{-i\hat{H}_{\rm total}t/\hbar}|\Psi_{\rm ne}\rangle - 1, \quad \text{(A7)}$$

$$P_{1,1}(t) = 2\langle\Psi_{\rm ne}|e^{i\hat{H}_{\rm total}t/\hbar}\left(\hat{S}_1^+\hat{S}_1^- - \tfrac{1}{2}\right)e^{-i\hat{H}_{\rm total}t/\hbar}|\Psi_{\rm ne}\rangle, \quad \text{(A8)}$$

$$P_{1,1}(t) = 2\langle\Psi_{\rm ne}|e^{i\hat{H}_{\rm total}t/\hbar}\hat{S}_1^ze^{-i\hat{H}_{\rm total}t/\hbar}|\Psi_{\rm ne}\rangle. \quad \text{(A9)}$$

Thus, the autocorrelation $P_{1,1}(t)$ written in the form of Eq. (A9) is, in fact, the expectation value of the $\hat{S}_1^z$ operator over the evolved nonequilibrium state $e^{-i\hat{H}_{\rm total}t/\hbar}|\Psi_{\rm ne}\rangle$. We note that an equivalent reasoning can be performed in the case of the local LE in Eq. (15) just replacing the forward propagator $e^{-i\hat{H}_{\rm total}t/\hbar}$ by the LE propagator $e^{-\frac{i}{\hbar}(-\hat{H}_{\mathcal{S}}+\hat{\Sigma})t_R}e^{-\frac{i}{\hbar}(\hat{H}_{\mathcal{S}}+\hat{\Sigma})t_R}$.

APPENDIX B: NUMERICAL SIMULATIONS WITH TROTTER-SUZUKI EVOLUTIONS

The computation of the time-dependent observable in Eq. (5) requires the evolution of each of the states participating in the ensemble. However, its implementation for large systems, e.g., by means of a fourth-order Trotter-Suzuki decomposition [44], soon becomes quite expensive in computational resources. Instead, the local nature of the excitation allows the employment of an algorithm exploiting the quantum parallelism [45] to give an exponential reduction of computational efforts. The evolution of a few pure states is enough to describe the ensemble-averaged excitation dynamics. Thus, a typical initial state representing the whole ensemble has the form

$$|\Psi\rangle = |\uparrow_1\rangle \otimes \left\{\sum_{r=1}^{2^{2m-1}}\frac{1}{\sqrt{2^{2m-1}}}e^{i\varphi_r}\ |\beta_r\rangle\right\}, \quad \varphi_r = \text{random phase}, \quad \text{(B1)}$$

which exploits the quantum superposition over the whole spin set. Typically, a few of these entangled states are enough to get rid of statistical noise and obtain local physical observables with a good accuracy. This highly efficient technique for spin-ensemble calculations is enhanced by the parallelization enabled by its implementation on a general-purpose graphical processing unit.

[1] C. H. Bennett and D. P. DiVincenzo, Nature **404**, 247 (2000).
[2] D. D. Awschalom and M. E. Flatté, Nat. Phys. **3**, 153 (2007).
[3] I. Bloch, J. Dalibard, and W. Zwerger, Rev. Mod. Phys. **80**, 885 (2008).
[4] J. F. Sherson, C. Weitenberg, M. Endres, M. Cheneau, I. Bloch, and S. Kuhr, Nature **467**, 68 (2010).
[5] L. Dicarlo, M. D. Reed, L. Sun, B. R. Johnson, J. M. Chow, J. M. Gambetta, L. Frunzio, S. M. Girvin, M. H. Devoret, and R. J. Schoelkopf, Nature **467**, 574 (2010).
[6] M. S. Grinolds, P. Maletinsky, S. Hong, M. D. Lukin, R. L. Walsworth, and A. Yacoby, Nat. Phys. **467**, 68 (2011).
[7] P. R. Levstein, G. Usaj, and H. M. Pastawski, J. Chem. Phys. **108**, 2718 (1998).
[8] H. M. Pastawski, P. R. Levstein, G. Usaj, J. Raya, and J. Hirschinger, Physica A **283**, 166 (2000).
[9] H. G. Krojanski and D. Suter, Phys. Rev. Lett. **93**, 090501 (2004).
[10] W. H. Zurek, F. M. Cucchietti, and J. P. Paz, Acta Phys. Pol. B **38**, 1685 (2007), and references therein.
[11] R. L. Kosut, A. Shabani, and D. A. Lidar, Phys. Rev. Lett. **100**, 020502 (2008).
[12] E. Knill and R. Laflamme, Phys. Rev. A **55**, 900 (1997).
[13] L. Viola, E. Knill, and S. Lloyd, Phys. Rev. Lett. **82**, 2417 (1999).
[14] C. A. Ryan, J. S. Hodges, and D. G. Cory, Phys. Rev. Lett. **105**, 200402 (2010), and references therein.
[15] G. A. Álvarez, A. Ajoy, X. Peng, and D. Suter, Phys. Rev. A **82**, 042306 (2010).
[16] T. D. Ladd, F. Jelezko, R. Laflamme, Y. Nakamura, C. Monroe, and J. L. O'Brien, Nature **464**, 45 (2010).
[17] S. Bose, Phys. Rev. Lett. **91**, 207901 (2003).

[18] Z. L. Mádi, B. Brutscher, T. Schulte-Herbrüggen, R. Brüschweiler, and R. R. Ernst, Chem. Phys. Lett. **268**, 300 (1997).
[19] P. Cappellaro, C. Ramanathan, and D. G. Cory, Phys. Rev. A **76**, 032317 (2007).
[20] W. Zhang, P. Cappellaro, N. Antler, B. Pepper, D. G. Cory, V. V. Dobrovitski, C. Ramanathan, and L. Viola, Phys. Rev. A **80**, 052323 (2009).
[21] E. Rufeil-Fiori, C. M. Sánchez, F. Y. Oliva, H. M. Pastawski, and P. R. Levstein, Phys. Rev. A **79**, 032324 (2009).
[22] E. B. Fel'dman and S. Lacelle, J. Chem. Phys. **107**, 7067 (1997).
[23] S. Doronin, I. Maksimov, and E. Fel'dman, J. Exp. Theor. Phys. **91**, 597 (2000).
[24] S. I. Doronin and E. B. Fel'dman, Solid State Nucl. Magn. **28**, 111 (2005).
[25] C. Ramanathan, P. Cappellaro, L. Viola, and D. G. Cory, New J. Phys. **13**, 103015 (2011).
[26] G. A. Álvarez, M. Mishkovsky, E. P. Danieli, P. R. Levstein, H. M. Pastawski, and L. Frydman, Phys. Rev. A **81**, 060302 (2010).
[27] P. Cappellaro, L. Viola, and C. Ramanathan, Phys. Rev. A **83**, 032304 (2011).
[28] H. M. Pastawski, P. R. Levstein, and G. Usaj, Phys. Rev. Lett. **75**, 4310 (1995).
[29] H. Pastawski, Chem. Phys. Lett. **261**, 329 (1996).
[30] V. N. Prigodin, B. L. Altshuler, K. B. Efetov, and S. Iida, Phys. Rev. Lett. **72**, 546 (1994).
[31] G. A. Álvarez, E. P. Danieli, P. R. Levstein, and H. M. Pastawski, Phys. Rev. A **82**, 012310 (2010).
[32] R. A. Jalabert and H. M. Pastawski, Phys. Rev. Lett. **86**, 2490 (2001).
[33] C. M. Sánchez, P. R. Levstein, R. H. Acosta, and A. K. Chattah, Phys. Rev. A **80**, 012328 (2009).
[34] M. F. Andersen, A. Kaplan, T. Grünzweig, and N. Davidson, Phys. Rev. Lett. **97**, 104102 (2006).
[35] R. Schäfer, H.-J. Stöckmann, T. Gorin, and T. H. Seligman, Phys. Rev. Lett. **95**, 184102 (2005).
[36] P. Jacquod and C. Petitjean, Adv. Phys. **58**, 67 (2009).
[37] T. Gorin, T. Prosen, T. H. Seligman, and M. Znidaric, Phys. Rep. **435**, 33 (2006); A. Goussev, R. A. Jalabert, H. M. Pastawski, and D. Wisniacki, arXiv:1206.6348 [nlin.CD].
[38] V. V. Flambaum and F. M. Izrailev, Phys. Rev. E **64**, 026124 (2001).
[39] P. R. Levstein, H. M. Pastawski, and R. Calvo, J. Phys.: Condens. Matter **3**, 1877 (1991).
[40] S. Zhang, B. H. Meier, and R. R. Ernst, Phys. Rev. Lett. **69**, 2149 (1992).
[41] E. P. Danieli, H. M. Pastawski, and P. R. Levstein, Chem. Phys. Lett. **384**, 306 (2004).
[42] A. Abragam, *The Principles of Nuclear Magnetism*, *The International Series on Monographs on Physics* (Oxford University Press, Oxford, 1986).
[43] C. P. Slichter, *Principles of Magnetic Resonance*, *Springer Series in Solid State Sciences*, 2nd ed. (Springer, Berlin, 1980).
[44] M. Rieth and W. Schommers, *Handbook of Theoretical and Computational Nanotechnology: Quantum and Molecular Computing, Quantum Simulations*, *Nanotechnology Book Series* (American Scientific, Valencia, CA, 2006).
[45] G. A. Álvarez, E. P. Danieli, P. R. Levstein, and H. M. Pastawski, Phys. Rev. Lett. **101**, 120503 (2008).
[46] E. Lieb, T. Schultz, and D. Mattis, Ann. Phys. **16**, 407 (1961).
[47] E. P. Danieli, H. M. Pastawski, and G. A. Álvarez, Chem. Phys. Lett. **402**, 88 (2005).
[48] A. K. Khitrin and B. M. Fung, J. Chem. Phys. **111**, 7480 (1999).
[49] P. W. Anderson, Rev. Mod. Phys. **50**, 191 (1978).
[50] C. Petitjean and P. Jacquod, Phys. Rev. Lett. **97**, 124103 (2006).
[51] O. Bohigas and J. Flores, Phys. Lett. B **34**, 261 (1971).
[52] V. V. Flambaum, G. F. Gribakin, and F. M. Izrailev, Phys. Rev. E **53**, 5729 (1996); V. V. Flambaum and F. M. Izrailev, *ibid.* **55**, R13 (1997).
[53] P. Jacquod and D. L. Shepelyansky, Phys. Rev. Lett. **79**, 1837 (1997).
[54] B. Georgeot and D. L. Shepelyansky, Phys. Rev. Lett. **81**, 5129 (1998).
[55] L. F. Santos, F. Borgonovi, and F. M. Izrailev, Phys. Rev. Lett. **108**, 094102 (2012).
[56] V. V. Flambaum and F. M. Izrailev, Phys. Rev. E **61**, 2539 (2000).
[57] E. Rufeil-Fiori and H. M. Pastawski, Physica B **404**, 2812 (2009).
[58] E. Rufeil-Fiori and H. M. Pastawski, Braz. J. Phys. **36**, 844 (2006).
[59] P. Jacquod, P. Silvestrov, and C. Beenakker, Phys. Rev. E **64**, 055203 (2001); F. M. Cucchietti, C. H. Lewenkopf, and H. M. Pastawski, *ibid.* **74**, 026207 (2006).
[60] E. Rufeil-Fiori and H. M. Pastawski, Chem. Phys. Lett. **420**, 35 (2006).
[61] A. D. Dente, P. R. Zangara, and H. M. Pastawski, Phys. Rev. A **84**, 042104 (2011).
[62] S. Chakravarty and A. J. Leggett, Phys. Rev. Lett. **52**, 5 (1984).
[63] U. Weiss, Quantum Dissipative Systems, *Series in Modern Condensed Matter Physics* (World Scientific, Singapore, 2008).
[64] P. Blanchard, G. Bolz, M. Cini, G. F. de Angelis, and M. Serva, J. Stat. Phys. **75**, 749 (1994).
[65] K. Machida, H. Nakazato, S. Pascazio, H. Rauch, and S. Yu, Phys. Rev. A **60**, 3448 (1999).